ELSEVIER

# Photoluminescent macrocyclic Pd(II) and Pt(II) dimeric complexes with $Ph_2P-C{\equiv}C-PPh_2$ spacer

Dengfeng Xu, Hunter J. Murfee, Wytze E. van der Veer, Bo Hong *

*Department of Chemistry, University of California, Irvine, CA 92697-2025, USA*

## Abstract

The synthesis and characterization of macrocyclic Pd(II)/Pt(II) dimers and their monomeric precursors with diphosphine spacer $Ph_2P-C{\equiv}C-PPh_2$ ($C_2P_2$) are reported. Their excited-state properties, including solvent-dependent absorption, emission and quantum yield, are studied. When the solvent polarity increases, solvatochromic absorption band shifts to higher energy, emission maximum shifts to lower energy, and quantum yield decreases. In addition, the host–guest behavior of these new inorganic macrocycles is also reported here. © 2000 Elsevier Science S.A. All rights reserved.

*Keywords:* Photoluminescence; Inorganic macrocycles; Polyphosphines; Host–guest; Pd(II) and Pt(II) complexes

## 1. Introduction

Macrocyclic molecules based on transition metals (inorganic and organometallic cyclophanes) have recently emerged as the latest members of self-assembly supramolecular systems [1–8]. Using metal-directed self-assembly methodologies, macrocyclic molecular squares, rectangles or boxes with Pd(II), Pt(II) and Re(I) metal centers have been prepared and studied due to their potential applications in areas such as host–guest chemistry, molecular recognition and sensing, and modeling for biological systems [1–4]. Using the pre-assembled metal-based moieties and suitable multidentate bridging ligands (or spacers), two- and three-dimensional metallomacrocycles of diverse shapes and sizes can be prepared [1,9,10].

Among the inorganic cyclophanes that have been extensively studied, the molecules with Re(I) centers were reported to be photoresponsive [2]. In the recent work by Hupp and co-workers [2] the Pd(II)/Pt(II)-based moieties were found to be able to quench the Re(I) excited state via electron transfer. However, for macrocyclic complexes with Pd(II) and Pt(II) centers, photoluminescence and solvent-dependent ground-state and excited-state properties have not been fully investi-

gated. Furthermore, many of the inorganic cyclophanes were constructed using spacers with aromatic and pyridine-type linkage groups [1–3], and the use of other types of rigid bridging ligands in the construction of photoluminescent macrocyclic complexes has not been extensively studied. In this paper we report the use of ditopic phosphines, namely, $Ph_2P-C{\equiv}C-PPh_2$ ($C_2P_2$), in the preparation and the study of macrocyclic dimeric rectangles. The use of phosphines provides certain advantages since they are excellent coordinate ligands with various metal centers such as Re(I), Pd(II), Pt(II), Ru(II), Os(II), and Rh(II), etc. [5,11,12]. In this paper, synthesis and characterization of Pd(II)/Pt(II) monomeric precursors and macrocyclic dimers **1–5** with $C_2P_2$ are carried out. Room-temperature luminescence and lifetimes, solvent-dependent absorption, emission and quantum yields, as well as the host–guest properties of these new complexes are reported here.



(M = Pd, **1**; Pt, **2**)

(M = Pd, **3**; Pt, **4**)

**5**
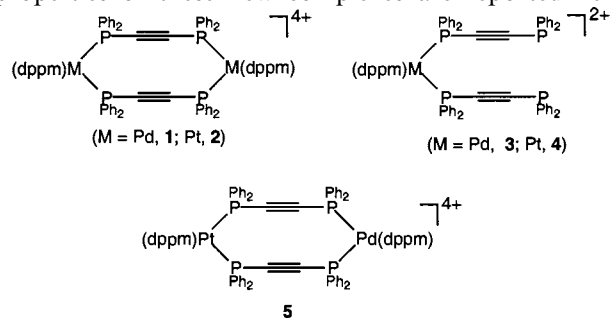
* Corresponding author.

*E-mail address:* bhong@uci.edu (B. Hong)

## 2. Experimental

### 2.1. General methods

All experiments were performed under a nitrogen atmosphere using standard glove box and Schlenk techniques.

### 2.2. Materials

(dppm)M(OTf)$_2$ [1b] (M = Pd, Pt), and Ph$_2$P–C≡C–PPh$_2$ (C$_2$P$_2$) [13] were prepared according to the literature methods. All spectrophotometric grade solvents were purchased from Fisher, dried over 4 Å molecular sieves for at least 24 h, and deoxygenated with dry N$_2$ for 20 min or longer prior to use. Acetonitrile (MeCN) was distilled under nitrogen over calcium hydride. HPLC grade CH$_2$Cl$_2$ was purchased from Fisher and deoxygenated with dry N$_2$ for 20 min or longer prior to use.

### 2.3. Physical measurements

#### 2.3.1. NMR study and elemental analysis

$^{31}$P{$^1$H}- and $^1$H-NMR spectra were obtained on an Omega 500 MHz spectrometer. The $^{31}$P{$^1$H}-NMR was referenced to a solution of 85% H$_3$PO$_4$ in D$_2$O. Combustion analysis (C and H) were measured with a Carlo Erba Instruments Fisons Elemental Analyzer.

#### 2.3.2. Mass spectral measurements

Fast atom bombardment mass spectra were recorded on a Micromass Autospec and electrospray mass spectra were recorded on a Micromass model LCT instrument at the UCI Mass Spectroscopy Laboratory. Representative fragments for complexes **1**–**5** are listed in Table 1.

#### 2.3.3. X-ray structure determination

A pale-yellow crystal of approximate dimensions

Table 1
FAB MS and ESI MS data for Pd(II) and Pt(II) complexes of C$_2$P$_2$

| Complex | ESI, $m/z$ [rel. %] | ESI assignment | FAB, $m/z$ [rel. %] | FAB assignment |
|---|---|---|---|---|
| **1** | 2216.7 [100] | [Pd(dppm)(C$_2$P$_2$)]$_2$(OTf)$_3^+$ | 2217.2 [100] | [Pd(dppm)(C$_2$P$_2$)]$_2$(OTf)$_3^+$ |
| | 2081.8 [40] | [Pd(dppm)(C$_2$P$_2$)]$_2$(OTf)$_2^+$ + 2O − F | 2082.3 [25] | [Pd(dppm)(C$_2$P$_2$)]$_2$(OTf)$_2^+$ + 2O − F |
| | 966.6 [30] | {[Pd(dppm)(C$_2$P$_2$)]$_2$(OTf) + O}$^{2+}$ | 2069.1 [45] | [Pd(dppm)(C$_2$P$_2$)]$_2$(OTf)$_2^+$ |
| | 958.5 [30] | [Pd(dppm)(C$_2$P$_2$)]$_2$(OTf)$^{2+}$ | 1919.5 [25] | [Pd(dppm)(C$_2$P$_2$)]$_2$(OTf)$^+$ |
| | 1882.8 [55] | [Pd(dppm)(C$_2$P$_2$)]$_2$(OTf)$^+$ − O − F | 1900.8 [20] | [Pd(dppm)(C$_2$P$_2$)]$_2$(OTf)$^+$ − F |
| | 1824.8 [40] | [Pd(dppm)(C$_2$P$_2$)]$_2^+$ + O + 2F | 1824.3 [30] | [Pd(dppm)(C$_2$P$_2$)]$_2^+$ + O + 2F |
| **2** | 2393.8 [100] | [Pt(dppm)(C$_2$P$_2$)]$_2$(OTf)$_3^+$ | 2393.5 [100] | [Pt(dppm)(C$_2$P$_2$)]$_2$(OTf)$_3^+$ |
| | 1047.5 [10] | [Pt(dppm)(C$_2$P$_2$)]$_2$(OTf)$^{2+}$ | 2243.7 [25] | [Pt(dppm)(C$_2$P$_2$)]$_2$(OTf)$_2^+$ |
| | 2059.8 [20] | [Pt(dppm)(C$_2$P$_2$)]$_2$(OTf)$^+$ − O − F | 2093.9 [25] | [Pt(dppm)(C$_2$P$_2$)]$_2$(OTf)$^+$ |
| | 972.0 [30] | [Pt(dppm)(C$_2$P$_2$)]$_2^{2+}$ | 1944.0 [60] | [Pt(dppm)(C$_2$P$_2$)]$_2^+$ |
| | 648.4 [15] | [Pt(dppm)(C$_2$P$_2$)]$_2^{3+}$ | | |
| **3** | 1463.1 [30] | [Pd(dppm)(C$_2$P$_2$)$_2$](OTf)$^+$ + O + F | 1535.0 [50] | [Pd(dppm)(C$_2$P$_2$)$_2$] (OTf)$_2^+$ + O − 3F |
| | 1448.1 [15] | [Pd(dppm)(C$_2$P$_2$)$_2$](OTf)$^+$ + F | 1300.0 [30] | [Pd(dppm)(C$_2$P$_2$)$_2$]$^+$ + F |
| | 1428.1 [5] | [Pd(dppm)(C$_2$P$_2$)$_2$](OTf)$^+$ | 1033.1 [100] | [Pd(dppm)(C$_2$P$_2$)](OTf)$^+$ |
| | 1327.1 [25] | [Pd(dppm)(C$_2$P$_2$)$_2$]$^+$ + 3O | 884.1 [98] | [Pd(dppm)(C$_2$P$_2$)]$^+$ |
| | 1279.1 [8] | [Pd(dppm)(C$_2$P$_2$)$_2$]$^+$ | | |
| | 1033.0 [100] | [Pd(dppm)(C$_2$P$_2$)](OTf)$^+$ | | |
| **4** | 1536.2 [5] | [Pt(dppm)(C$_2$P$_2$)$_2$](OTf)$^+$ + F | 1535.5 [5] | [Pt(dppm)(C$_2$P$_2$)$_2$](OTf)$^+$ + F |
| | 1517.2 [10] | [Pt(dppm)(C$_2$P$_2$)$_2$](OTf)$^+$ | 1384.2 [7] | [Pt(dppm)(C$_2$P$_2$)$_2$]$^+$ + O |
| | 1367.2 [5] | [Pt(dppm)(C$_2$P$_2$)$_2$]$^+$ | 1367.3 [15] | [Pt(dppm)(C$_2$P$_2$)$_2$]$^+$ |
| | 683.6 [95] | [Pt(dppm)(C$_2$P$_2$)$_2$]$^{2+}$ | 1122.1 [100] | [Pt(dppm)(C$_2$P$_2$)](OTf)$^+$ |
| | 1122.1 [100] | [Pt(dppm)(C$_2$P$_2$)](OTf)$^+$ | 973.1 [96] | [Pt(dppm)(C$_2$P$_2$)]$^+$ |
| **5** | 2306.7 [100] | [PtPd(dppm)$_2$(C$_2$P$_2$)$_2$](OTf)$_3^+$ | 2321.8 [25] | [PtPd(dppm)$_2$(C$_2$P$_2$)$_2$](OTf)$_3^+$ + O |
| | 2006.3 [5] | [PtPd(dppm)$_2$(C$_2$P$_2$)$_2$](OTf)$^+$ | 2305.6 [100] | [PtPd(dppm)$_2$(C$_2$P$_2$)$_2$](OTf)$_3^+$ |
| | 1928.5 [15] | [PtPd(dppm)$_2$(C$_2$P$_2$)$_2$](OTf)$^+$ − Ph | 2171.5 [30] | [PtPd(dppm)$_2$(C$_2$P$_2$)$_2$](OTf)$_2^+$ + O |
| | 1892.6 [5] | [PtPd(dppm)$_2$(C$_2$P$_2$)$_2$]$^+$ + O + F | 2156.6 [40] | [PtPd(dppm)$_2$(C$_2$P$_2$)$_2$](OTf)$_2^+$ |
| | | | 2005.6 [60] | [PtPd(dppm)$_2$(C$_2$P$_2$)$_2$](OTf)$^+$ |

$0.20 \times 0.17 \times 0.10$ mm$^3$ was mounted on a glass fiber and transferred to a Bruker CCD platform diffractometer. The SMART [14a] program package was used to determine the unit-cell parameters and for data collection (30 s/frame counting time for a hemisphere of diffraction data). The raw frame data were processed using SAINT [14b] and SADABS [14c] to yield the reflection data file. Subsequent calculations were carried out using the SHELXTL [14d] program. The systematic absences were consistent with the triclinic space group $P\bar{1}$.

The structure was solved by direct methods and refined on $F^2$ by full-matrix least-squares techniques. The analytical scattering factors [14e] for neutral atoms were used throughout the analysis. There are two cations per unit cell. All atoms of the cations were refined anisotropically; isotropic displacement parameters were employed for the remaining atoms. Hydrogen atoms were not included in the refinement. The triflate group containing S4 is disordered about an inversion center and was refined as equal proportions of the two components. Atoms O13 through O17 were assumed to be oxygen atoms though the evidence is not definitive. This model is one unit of negative charge short of charge balance (two $+4$ cations and seven triflate anions per unit cell). At convergence, $R_1 = 0.0692$, $wR_2 = 0.1755$ and GoF = 1.070 for 1156 variables refined against 19 407 unique data.

### 2.3.4. Photophysical measurements

Absorption spectra were recorded on a Hewlett–Packard 8453 diode array spectrophotometer. Steady-state emission spectra were obtained on a Hitachi F-4500 fluorescence spectrometer. Luminescence quantum yields of all complexes were measured relative to Ru(bpy)$_3$(PF$_6$)$_2$ ($\Phi = 0.062$ in acetonitrile [15]) after being deoxygenated using three freeze–pump–thaw processes.

The lifetime values were obtained with a Fourier transform spectrofluorometer, SLM — Aminco 48000 MHF. As a light source the 476.5 nm line of a Coherent Innova 90 argon ion laser was used. The laser beam was modulated with a comb function with an interval spacing of 5 MHz; the maximum frequency is 250 MHz. The resulting beam was imaged on the sample; the resulting luminescence was detected with a photomultiplier via a Schott filter (OG 515 or OG 530). The phase and intensity of each component of the comb function were determined; the required reference signal was obtained by picking off a small part of the beam incident on the sample. The resulting signals were fitted with a single exponential, obtaining the best fit with respect to both the recorded phase and intensity information. For each sample a series of five measurements was obtained, each consisting of 1000 scans.

### 2.4. General preparation of macrocyclic dimeric Pd(II) and Pt(II) complexes (1, 2)

A solution of M(dppm)(OTf)$_2$ (M = Pd, Pt) and C$_2$P$_2$ (0.1 mmol, 1:1 ratio) in 20 ml of methylene chloride was stirred for 2 h. The solvent was removed via vacuum evaporation. The residue thus obtained was re-dissolved in a minimum amount of CH$_2$Cl$_2$, and added dropwise to diethyl ether (50 ml). The yellow precipitate was collected by vacuum filtration, washed with diethyl ether (3 × 10 ml), and then dried in vacuo.

#### 2.4.1. [(dppm)Pd(C$_2$P$_2$)]$_2$(OTf)$_4$ (1)

Yield: 95%. $^{31}$P{$^1$H}-NMR (202.4 MHz, acetone-$d_6$): $\delta$ $-3.28$ ppm (d, dppm, $^2J_{P-P} = 348$ Hz), $-26.80$ ppm (d, C$_2$P$_2$, $^2J_{P-P} = 348$ Hz). $^1$H-NMR (500 MHz, acetone-$d_6$): $\delta$ 5.61 ppm (s, $-$CH$_2-$, 4H), 7.09–7.71 ppm (m, Ph, 80H). Anal. Calc. for **1** (Pd$_2$C$_{106}$H$_{84}$O$_{12}$S$_4$P$_8$F$_{12}$): C% 53.80, H% 3.58; found: C% 53.62, H% 3.80.

#### 2.4.2. [(dppm)Pt(C$_2$P$_2$)]$_2$(OTf)$_4$ (2)

Yield: 96%. $^{31}$P{$^1$H}-NMR (202.4 MHz, acetone-$d_6$): $\delta$ $-10.19$ ppm (d, dppm, $^2J_{P-P} = 318$ Hz, Pt satellites, $^1J_{Pt-P} = 1274$ Hz), $-35.60$ ppm (d, C$_2$P$_2$, $^2J_{P-P} = 318$ Hz, Pt satellites, $^1J_{Pt-P} = 1068$ Hz). $^1$H-NMR (500 MHz, acetone-$d_6$): $\delta$ 5.61 ppm (s, $-$CH$_2-$, 4H), 7.11–7.84 ppm (m, Ph, 80H). Anal. Calc. for **2** (Pt$_2$C$_{106}$H$_{84}$O$_{12}$S$_4$P$_8$F$_{12}$): C% 50.05, H% 3.33; found: C% 49.56, H% 3.41.

### 2.5. General preparation of monomeric Pd(II) and Pt(II) complexes (3, 4)

A solution of M(dppm)(OTf)$_2$ (M = Pd, Pt, 0.1 mmol) and C$_2$P$_2$ (0.3 mmol) in 30 ml of acetonitrile was stirred for 20 h. The solvent was removed with a cold finger, and the residue was re-dissolved in a minimum amount of acetonitrile and added dropwise to diethyl ether (50 ml). The yellow precipitate was collected by vacuum filtration, washed with diethyl ether (3 × 10 ml), and then dried in vacuo.

#### 2.5.1. [(dppm)Pd(C$_2$P$_2$)$_2$](OTf)$_2$ (3)

Yield: 64%. $^{31}$P{$^1$H}-NMR (202.4 MHz, acetone-$d_6$): $\delta$ $-3.16$ ppm (d, dppm, $^2J_{P-P} = 342$ Hz), $-24.57$ ppm (d, Pd$-$P$-$C≡C, $^2J_{P-P} = 342$ Hz), $-29.60$ ppm (s, P$-$C≡C). $^1$H-NMR (500 MHz, acetone-$d_6$): $\delta$ 5.61 ppm (s, $-$CH$_2-$, 2H), 7.15–7.55 ppm (m, Ph, 60H). Anal. Calc. for **3** (PdC$_{79}$H$_{62}$O$_6$S$_2$P$_6$F$_6$): C% 60.14, H% 3.96; found: C% 60.56, H% 4.00.
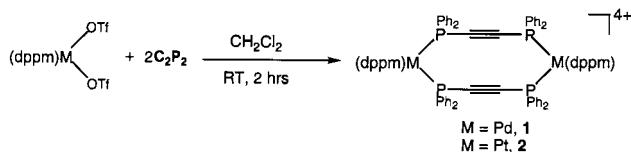
Scheme 1.
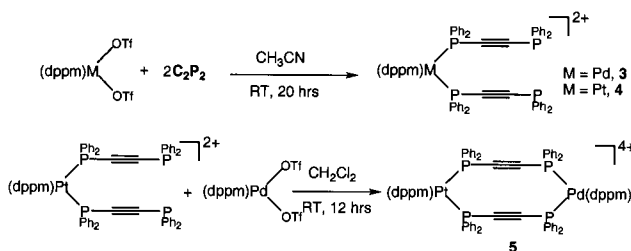


Scheme 2.

### 2.5.2. [(dppm)Pt(C₂P₂)₂](OTf)₂ (4)

Yield: 53%. $^{31}$P{$^{1}$H}-NMR (202.4 MHz, acetone-$d_6$): $\delta$ − 8.49 ppm (d, dppm, $^{2}J_{P-P}$ = 311 Hz, Pt satellites, $^{1}J_{Pt-P}$ = 1225 Hz), − 32.99 ppm (d, Pt−P−C≡C, $^{2}J_{P-P}$ = 311 Hz, Pt satellites, $^{1}J_{Pt-P}$ = 1017 Hz), − 29.60 ppm (s, P−C≡C). $^{1}$H-NMR (500 MHz, acetone-$d_6$): $\delta$ 5.47 ppm (s, −CH₂−, 2H), 7.20−7.64 ppm (m, Ph, 60H). Anal. Calc. for 4 (PtC₇₉H₆₂O₆S₂P₆F₆): C% 56.94, H% 3.75; found: C% 56.45, H% 4.16.

### 2.6. General preparation of mixed-metal macrocyclic dimeric complexes (5)

A solution of [(dppm)Pt(C₂P₂)₂](OTf)₂ (4) and Pd(dppm)(OTf)₂ (0.033 mmol, 1:1 ratio) in 30 ml of CH₂Cl₂ was stirred at room temperature for 12 h. The solvent was removed by vacuum evaporation. The resulting residue was re-dissolved in a minimum amount of CH₂Cl₂, and added dropwise to diethyl ether (50 ml). The precipitate was collected by vacuum filtration, washed with diethyl ether (3 × 10 ml), and then dried in vacuo.

### 2.6.1. [(dppm)Pd(C₂P₂)₂Pt(dppm)](OTf)₄ (5)

Yield: 84%. $^{31}$P{$^{1}$H-NMR (202.4 MHz, acetone-$d_6$): $\delta$ − 2.79 ppm (d, Pd−P−CH₂, $^{2}J_{P-P}$ = 348 Hz), − 10.31 ppm (d, Pt−P−CH₂, $^{2}J_{P-P}$ = 318 Hz, Pt satellites, $^{1}J_{Pt-P}$ = 1274 Hz), − 27.50 ppm (d, Pd−P−C≡C, $^{2}J_{P-P}$ = 348 Hz), − 34.87 ppm (d, Pt−P−C≡C, $^{2}J_{P-P}$ = 318 Hz, Pt satellites, $^{1}J_{Pt-P}$ = 1068 Hz). $^{1}$H-NMR (500 MHz, acetone-$d_6$): $\delta$ 5.61 ppm (s, −CH₂−P−Pd, 2H), 5.41 ppm (s, −CH₂−P−Pt, 2H), 7.18−7.68 ppm (m, Ph, 80H). Anal. Calc. for 5 (PtPdC₁₀₆H₈₄O₁₂S₄P₈F₁₂): C% 51.85, H% 3.45, found: C% 51.84, H% 3.75.

## 3. Results and discussion

### 3.1. Synthesis

The synthesis of homobimetallic Pd(II) and Pt(II) macrocycles (1 and 2) was straightforward (Scheme 1). M(dppm)(OTf)₂ (M = Pd or Pt) and C₂P₂ (1:1 molar ratio) were mixed together in CH₂Cl₂ to give products in excellent yields. Typically, dimeric complexes were the predominant products despite the amount of solvent used and the purity of products was established using NMR and elemental analysis.

The heterobimetallic macrocycle 5 with C₂P₂ was synthesized from monomeric precursor 4 and one equivalent of Pd(dppm)(OTf)₂ (Scheme 2). A couple of interesting features existed in the synthesis. First, CH₃CN was found to be a better solvent than CH₂Cl₂ in the synthesis of monomeric complex 4. Reaction between M(dppm)(OTf)₂ (M = Pd or Pt) and C₂P₂ in CH₂Cl₂ gave homobimetallic complex 1 or 2 as the predominant product. Secondly, Pt(II)-based monomer 4 was used to prepare the heterobimetallic complex 5. When [Pd(dppm)(C₂P₂)₂](OTf)₂ (3) was used to react with Pt(dppm)(OTf)₂, a mixture of Pd(II) and Pt(II) homo- and heterobimetallic complexes was always obtained.

### 3.2. Characterization

$^{1}$H- and $^{31}$P{$^{1}$H}-NMR, X-ray structure determination, fast atom bombardment (FAB) and electrospray (ESI) mass spectral study, and elemental analysis were used in the characterization of the dimeric macrocycles and their monomeric precursors. In the $^{31}$P{$^{1}$H}-NMR analysis, it was observed that the homobimetallic complexes always gave two doublets, as listed in Section 2, due to the coupling between the P atoms in C₂P₂ and dppm. Fig. 1(a) gives a representative spectrum for [Pt(dppm)(C₂P₂)]₂(OTf)₄ (2), with one doublet at − 10.19 ppm for dppm and another at − 35.60 ppm for C₂P₂. The $^{2}J_{P-P}$ coupling constant between the phosphorus atoms in dppm and C₂P₂ in 2 is 318 Hz. For other complexes reported here, such $^{2}J_{P-P}$ coupling constant is in the range of 311−348 Hz, characteristic of the expected large $J_{P-P}$ coupling constant between trans phosphorus atoms on the same metal center [11]. In addition, for all complexes with Pt(II) centers, the Pt(II) satellites were also observed with the $^{1}J_{Pt-dppm}$ coupling constant in the range of 1225−1274 Hz (between Pt and dppm) and $^{1}J_{Pt-C_2P_2}$ in the range of 1017−1068 Hz (between Pt and C₂P₂). Heterobimetallic complex 5 gives four doublets (Fig. 1(b)). Two of them are from phosphines on the Pd(II) center (− 2.79 ppm for dppm and − 27.50 ppm for C₂P₂), and the other two from the Pt(II) side (− 10.31 ppm for dppm and − 34.87 ppm for C₂P₂). Pt(II) satellites were also ob-

served with $^1J_{Pt-dppm}$ of 1274 Hz and $^1J_{Pt-C_2P_2}$ of 1068 Hz. For monomeric complexes two doublets (from dppm and the coordinated P atom of $C_2P_2$) and one singlet (corresponding to the uncoordinated P atom of $C_2P_2$) were observed. For the latter the same chemical shift at −29.60 ppm was found in both complexes **3** and **4**.

The determination of structures and relative molecular masses of macrocycles has posed a great challenge in the field of metal-containing cyclophanes and supramolecules [1–3]. Single-crystal structure determination can provide direct evidence regarding the metal-to-metal distance and the cavity size. A single crystal of dimensions $0.20 \times 0.17 \times 0.10$ mm$^3$ was used for data collection at 158 K for complex **2**. The pertinent crystallographic information is listed in Table 2. The compound crystallizes in the space group $P\bar{1}$ with two molecules per unit cell. As shown in Fig. 2, a ten-member ring, consisting of two Pt centers and two $C_2P_2$ spacers, is formed in the cation $[(dppm)Pt(C_2P_2)]_2^{4+}$, with a Pt–Pt distance of 7.2 Å. Interestingly, the bond angles P(3)–Pt(1)–P(4) (94.07 (9)°) and P(7)–Pt(2)–P(8) (93.48 (9)°) are much greater than the angles P(1)–Pt(1)–P(2) (70.09 (10)°) and P(5)–Pt(2)–P(6) (70.63 (10)°). Presumably this is caused by the different constraint within the four-member ring (with dppm) and the ten-member ring (with $C_2P_2$). A slightly bent

Table 2
Crystal data and structure refinement

| Complex | **2** |
| --- | --- |
| Empirical formula | $Pt_2P_8C_{102}H_{84} \cdot 3.5OTf$ [a] |
| Formula weight | 2559.46 |
| Crystal system | Triclinic |
| Space group | $P\bar{1}$ |
| Wavelength (Å) | 0.71073 |
| Temperature (K) | 158 (2) |
| $a$ (Å) | 15.7454 (7) |
| $b$ (Å) | 16.1611 (7) |
| $c$ (Å) | 25.5260 (12) |
| $\alpha$ (°) | 79.6390 (10) |
| $\beta$ (°) | 78.7170 (10) |
| $\gamma$ (°) | 62.2690 (10) |
| Volume (Å$^3$) | 5608.7 (4) |
| $Z$ | 2 |
| $F(000)$ | 2555 |
| $\rho_{calc}$ (Mg m$^{-3}$) | 1.516 |
| $\mu$ (mm$^{-1}$) | 2.748 |
| Crystal size (mm$^3$) | $0.20 \times 0.17 \times 0.10$ |
| Reflections collected | 46886 |
| Independent reflections | 19407 [$R_{int} = 0.0474$] |
| $S (F^2)$ [b] | 1.070 |
| Final $R$ indices [c] [$I > 2\sigma(I)$] | $R_1 = 0.0692$, $wR_2 = 0.1755$ |
| $R$ indices (all data) [c] | $R_1 = 0.0950$, $wR_2 = 0.1894$ |

[a] Please refer to the discussions regarding the structural determination of complex **2**.

[b] $S$ = goodness of fit = $[\Sigma [w(F_o^2 - F_o^2)^2] = (n-p)]^{1/2}$, where $n$ is the number of reflections and $p$ is the total number of parameters refined.

[c] $R_1 = \Sigma ||F_o| - |F_c|| = \Sigma |F_o|$ and $wR_2 = [\Sigma [w(F_o^2 - F_o^2)^2] = \Sigma [w(F_o^2)^2]^{1/2}$, $w = 1/\sigma^2(|F_o|)$.
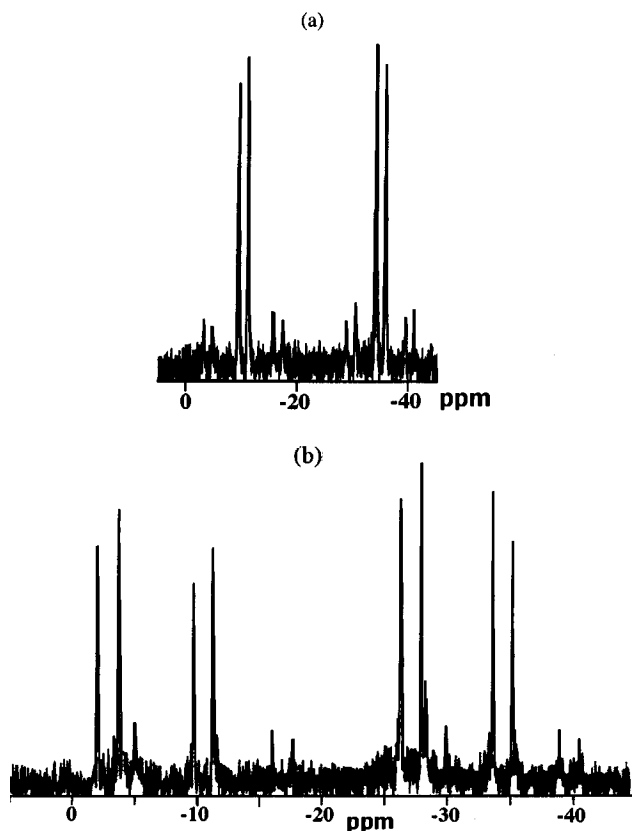


(a)



(b)

Fig. 1. $^{31}P\{^1H\}$-NMR spectra for (a) $[(dppm)Pt(C_2P_2)]_2(OTf)_4$ (**2**) and (b) $[(dppm)Pd(C_2P_2)Pt(dppm)]$ (**5**).
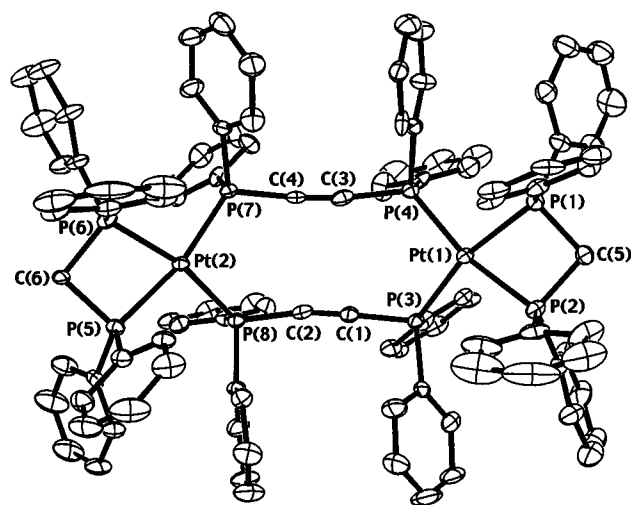


Fig. 2. ORTEP of the cation of **2**.

'linear' arrangement is observed for both P(3)–C(1)–C(2)–P(8) and P(4)–C(3)–C(4)–P(7). Selected bond lengths and angles are listed in Table 3.

Since there are two cations with a total of 8 + charges per unit cell, we should observe a total of eight

$OTf^-$ counteranions within each unit cell. However, the current structural model is one unit of negative charge short of charge balance (two $+4$ cations and seven triflate anions per unit cell). At convergence, $R_1 = 0.0692$, $wR_2 = 0.1755$ and GoF $= 1.070$ for 1156 variables refined against 19 407 unique data.

In addition to the use of X-ray structure determination, both FAB MS and ESI MS analysis are found to be useful techniques in the identification of macrocyclic complexes. Table 1 lists the representative high-molecular-weight fragments for complexes **1–5**, and Fig. 3 shows the FAB mass spectrum of **2** and the isotope distributions for fragment $(2–OTf)^+$ ($m/z = 2393.8$) in the ESI MS analysis. It was observed that the typical fragmentation pattern in the high-molecular-weight region involves the consecutive loss of the $OTf^-$ counteranions, leaving the innersphere metal–phosphine coordination intact (Fig. 3(a)). Importantly, the calculated and experimental isotopic distributions of fragment $(2–OTf)^+$ are in excellent agreement and in accord with the expected $m/z$ separation of 1 $m/z$ unit (Fig. 3(b)). Such features have also been observed in the mass spectral analysis of other monomeric and dimeric complexes (Table 1). Furthermore, the addition and loss of extra O and/or F atoms have been observed. For FAB MS analysis, all fragments have one positive charge. However, although the majority of the fragments were found to bear one positive charge, fragments with two positive charges were also observed in ESI MS analysis. For example, the fragments $(M–3OTf)^{2+}$ and $(M–4OTf)^{2+}$ were found for the ESI MS analysis of complexes **1** and **2**. All these mass spectral data, together with the $^1$H- and $^{31}$P{$^1$H}-NMR and elemental analysis, provide straightforward identification of our new monomeric and macrocyclic complexes with polyphosphines.

Table 3
Selected bond distances (Å) and bond angles (°) for complex **2**

| Bond distances | | | |
|---|---|---|---|
| Pt(1)–P(1) | 2.353 (3) | Pt(1)–P(2) | 2.326 (3) |
| Pt(1)–P(3) | 2.327 (3) | Pt(1)–P(4) | 2.333 (3) |
| Pt(2)–P(5) | 2.349 (3) | Pt(2)–P(6) | 2.338 (3) |
| Pt(2)–P(7) | 2.337(3) | Pt(2)–P(8) | 2.326 (3) |
| P(3)–C(1) | 1.739 (11) | P(4)–C(3) | 1.774 (12) |
| P(7)–C(4) | 1.754 (12) | P(8)–C(2) | 1.743 (12) |
| C(1)–C(2) | 1.223 (15) | C(3)–C(4) | 1.200 (16) |
| | | | |
| Bond angles | | | |
| P(2)–Pt(1)–P(1) | 70.09 (10) | P(3)–Pt(1)–P(4) | 94.07 (9) |
| P(2)–Pt(1)–P(3) | 97.03 (10) | P(2)–Pt(1)–P(4) | 167.62 (10) |
| P(3)–Pt(1)–P(1) | 165.40 (10) | P(4)–Pt(1)–P(1) | 98.18 (9) |
| P(8)–Pt(2)–P(7) | 93.48 (9) | P(8)–Pt(2)–P(6) | 166.82 (10) |
| P(7)–Pt(2)–P(6) | 98.53 (10) | P(8)–Pt(2)–P(5) | 96.89 (9) |
| P(7)–Pt(2)–P(5) | 168.06 (10) | P(6)–Pt(2)–P(5) | 70.63 (10) |
| C(1)–C(2)–P(8) | 169.3 (10) | C(2)–C(1)–P(3) | 175.7 (10) |
| C(4)–C(3)–P(4) | 172.9 (10) | C(3)–C(4)–P(7) | 175.1 (10) |
| P(2)–C(5)–P(1) | 94.0 (5) | P(5)–C(6)–P(6) | 94.5 (5) |
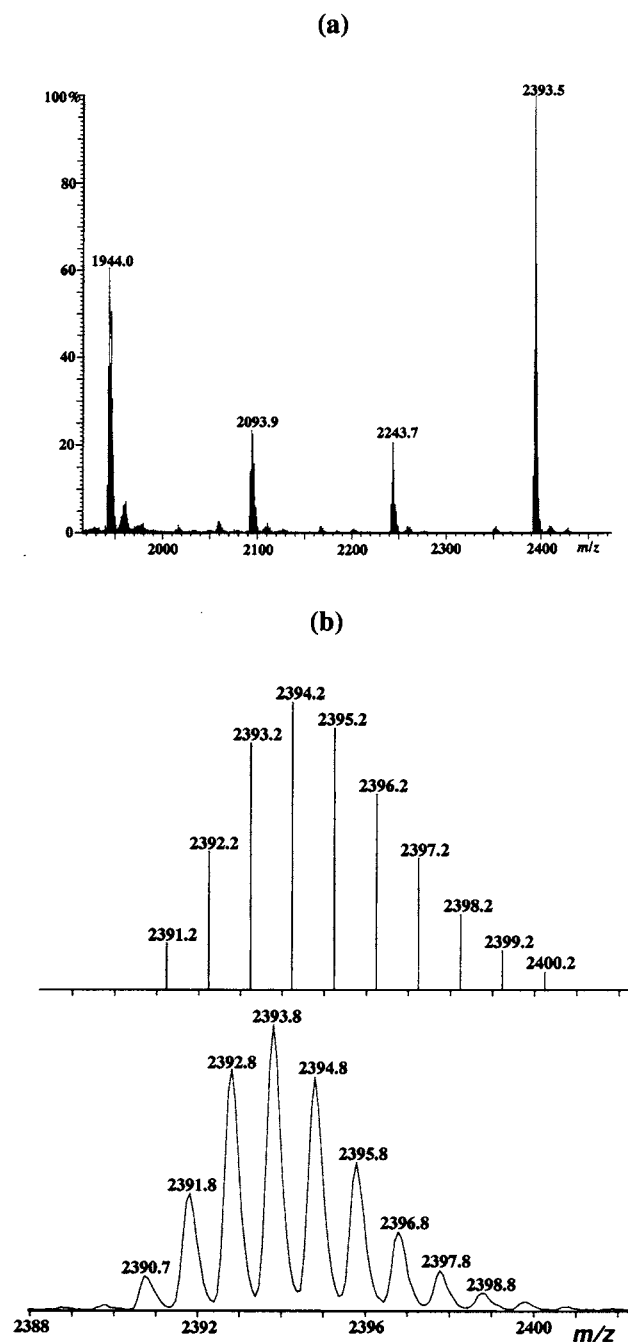


Fig. 3. (a) FAB mass spectrum of **2**. (b) Simulated (top) and observed (bottom) isotope distribution of fragment $(2\text{-}OTf)^+$ in ESI MS analysis.

### 3.3. Electronic absorption, emission, quantum yield and their solvent dependence

All new Pd(II) and Pt(II) complexes with dppm and $C_2P_2$ spacer were found to be emissive at room temperature. Table 4 compares the representative data of the ground-state absorption, excited-state emission and quantum yield of complexes **1–5**. Previously the synthesis and the structure determination of dimeric macro-

cyclic complexes with the formula $[X_2M(C_2P_2)_2MX_2]$ (M = Pd, Pt; X = Cl, Br and I) were reported [5b–d]. However, no absorption and emission properties were observed or studied.

For the ground-state electronic absorption, the monomeric and bimetallic complexes with Pd(II) centers exhibit intense charge transfer (CT) absorption bands between 345 and 352 nm in $CH_2Cl_2$ ($\varepsilon = 27\,190$–$62\,150$ $M^{-1}$ $cm^{-1}$), and the corresponding ones with Pt(II) centers show stronger absorption peaks at higher energy level (272–275 nm with $\varepsilon = 41\,890$–$95\,375$ $M^{-1}$ $cm^{-1}$). Such a blue shift in the CT band of the Pt(II)–phosphine complex versus the Pd(II)–phosphine complex has been reported in the Pt(II)/Pd(II) species with phosphines such as 1,2-bis(diphenylphosphino)benzene and 1,2,4,5-tetrakis(diphenylphosphino)benzene [12c]. Correspondingly, the emission maxima of the complexes with Pd(II) are between 530 and 532 nm while blue-shifted emission maxima at 512-518 nm were observed for the corresponding Pt(II) complexes. Some additional features are observed regarding the photophysical measurements. (i) The absorption extinction coefficients and quantum yields of the homobimetallic complexes 1 and 2 are approximately twice of that of the corresponding monomers 3 and 4. (ii) Mono- and homobimetallic Pt(II) complexes have higher quantum yields than the corresponding Pd(II) complexes. (iii) Excitation at 450 nm of 5 in $CH_2Cl_2$ results in the appearance of luminescence centered at 530 nm. This peak is assigned to the Pd(II)* emitting excited state based on the observed emission maxima of the monomeric and homobimetallic complexes 1–4. Possible energy transfer from the Pt(II) to Pd(II) center may exist in the heterobimetallic macrocycle 5. Following the conventional assumptions [16–18], the free-energy change $\Delta G°$ of energy transfer can be expressed as the difference between the spectroscopic energies of the energy donor and acceptor. The actual calculated value is 734 $cm^{-1}$ or 0.09 eV between the Pd- and Pt-based units, estimated from the energy of the emission maxima of homobimetallic complexes 1 and 2. When such energy transfer is efficient, the dominating emission of 5 will be from the Pd(II)* excited state.

Luminescence lifetimes of the monomeric and bimetallic complexes with $C_2P_2$ were measured using phase-modulated emission measurements. The monomeric Pd(II) and Pt(II) complexes 3 and 4 have lifetimes of 3.6 and 2.3 ns, respectively. Both homobimetallic complexes 1 and 2 exhibit shorter lifetimes ($\tau = 1.00$ ns for both 1 and 2) when compared with the corresponding monomeric species. For heterobimetallic complex 5, only the lifetime at 2.8 ns was observed, corresponding to the Pd-based excited state. No component of the lifetime corresponding to the quenched Pt(II)-based excited state was detected on the phase-modulated system within the measurable range of 500 ps to 200 ns. Presumably, the lifetime of the Pt-based excited state is shorter than 500 ps due to the energy transfer from the Pt(II)-based chromophore to the Pd(II)-based one.

Solvent dependence of the absorption, emission and quantum yield was also studied. For electronic absorption, both dimeric complexes 1 and 2 were found to have significant solvent-induced shifts in the visible region in the solvatochromic measurements, with a relative larger shift in the absorption peak maximum of 1 (Table 5). As compared in Fig. 4, the absorption maximum of the CT band of 1 shifts to a higher energy when the solvents are changed from THF and $CH_2Cl_2$ to DMF, $CH_3CN$, and DMSO that have higher polarity. Presumably the solvents with higher polarity may stabilize the ground state and, hence, increase the en-

Table 4
Photophysical data for 1–5

| Complex | Absorption maximum ($\lambda_{abs}$, nm) [a] | Extinction coefficient ($\varepsilon$, $M^{-1}$ $cm^{-1}$) | Emission maximum ($\lambda_{em}$, nm) [b] | Quantum yield [b] ($\times 10^{-4}$) | Lifetime [c] (ns) |
|---|---|---|---|---|---|
| $[(dppm)Pd(C_2P_2)]_2(OTf)_4$ (1) | 350 | 62 150 | 532 | 59 | $1.0 \pm 0.1$ |
| $[(dppm)Pt(C_2P_2)]_2(OTf)_4$ (2) | 273 | 95 375 | 512 | 400 | $1.0 \pm 0.1$ |
| $[(dppm)Pd(C_2P_2)_2](OTf)_2$ (3) | 345 | 29 440 | 530 | 34 | $3.6 \pm 0.4$ |
| $[(dppm)Pt(C_2P_2)_2](OTf)_2$ (4) | 272 | 41 890 | 518 | 230 | $2.3 \pm 0.2$ |
| $[(dppm)Pd(C_2P_2)_2Pt(dppm)](OTf)_4$ (5) | 275, 352 | 49 820, 27 190 | 530 | 90 | $2.8 \pm 0.3$ [d] |

[a] Measured in $CH_2Cl_2$.
[b] Excited at 450 nm in $CH_2Cl_2$.
[c] The sample was irradiated with the 476.5 nm line of the Ar laser. The luminescence signal was detected with a OG 515 or OG 530 filter.
[d] The lifetime of the quenched Pt(II)-based excited state was not observed on the phase-modulated emission spectrometer (measurable range 500 ps–200 ns).

Table 5
Absorption maxima ($\lambda_{abs}$, nm) and extinction coefficient ($\varepsilon$, $M^{-1}$ $cm^{-1}$) in different solvents

| Solvent | $\lambda_{abs}$ ($\varepsilon$, $M^{-1}$ $cm^{-1}$) for 1 | $\lambda_{abs}$ ($\varepsilon$, $M^{-1}$ $cm^{-1}$) for 2 |
|---|---|---|
| $CH_2Cl_2$ | 350 (62 150) | 273 (95 375) |
| THF | 352 (53 760) | 274 (76 960) |
| $CH_3CN$ | 330 (42 350) | 272 (76 850) |
| DMSO | 323 (46 070) | 270 (74 480) |
| DMF | 319 (23 200) | 270 (59 460) |
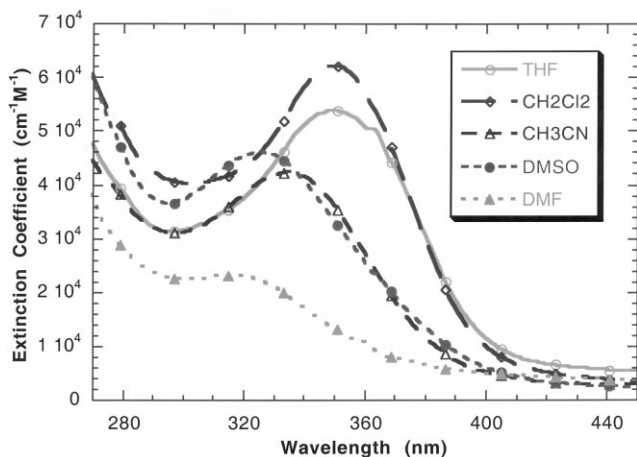


Fig. 4. Solvent-induced shift in electronic absorption maxima of [(dppm)Pd(C$_2$P$_2$)]$_2$(OTf)$_4$ (1).
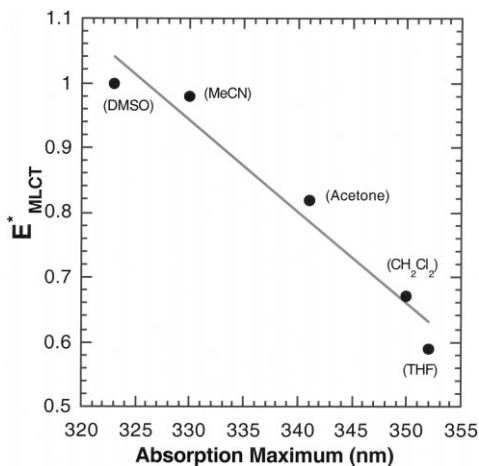


Fig. 5. Correlation between CT band absorption maxima of [(dppm)Pd(C$_2$P$_2$)]$_2$(OTf)$_4$ (1) and the $E^*_{MLCT}$ solvent scale.

ergy of the CT absorption band [19–21]. A plot of the energies of the CT band maxima versus solvent parameter gave an excellent correlation using Lee's $E^*_{MLCT}$ solvent scale [21] (Fig. 5). Previously, Lee's $E^*_{MLCT}$ solvent scale has been used by Cummings and Eisenberg [19d] in the study of the correlation and the solvatochromic effect in the Pt(II)/dithiolate systems.

The excited-state emission of both 1 and 2 was also found to have a strong dependence on solvents (Table 6). As shown in Fig. 6, upon changing from $CH_2Cl_2$ to DMSO the emission intensity of [(dppm)-Pt(C$_2$P$_2$)]$_2$(OTf)$_4$ (2) decreases significantly, and the emission maximum shifts to lower energy (from $\lambda_{em} = 512$ nm in $CH_2Cl_2$ to $\lambda_{em} = 525$ nm in DMSO). It was reported that larger Stokes shift values were observed when solvents with higher polarity were used in the absorption and emission measurements: $\Delta f \propto (u^* - u)^2$, where $\Delta f$ is the Stokes shift, and ($u^* - u$) is the dipole moment change upon excitation [20]. In our macrocyclic systems, a blue shift in the absorption and a red shift in the corresponding emission were observed when the solvent polarity increases, giving larger Stokes shift measured in the solvents with higher polarity. Corresponding to the changes in the emission maxima as a function of solvent polarity, the quantum yields change dramatically, especially in cyclophane 2. A 24-fold decrease was observed when the solvent was changed from $CH_2Cl_2$ to DMF with higher polarity. As shown in Fig. 7, a very good correlation was also observed between Lee's $E^*_{MLCT}$ solvent scale and the quantum yields of 2 in different solvents.

Table 6
Solvent-dependent emission [a] and quantum yield

| Solvent | $\lambda_{em}$ (nm) ($\Phi$, $\times 10^{-4}$) for 1 | $\lambda_{em}$ (nm) ($\Phi$, $\times 10^{-4}$) for 2 |
|---|---|---|
| $CH_2Cl_2$ | 532 (59) | 512 (400) |
| THF | 532 (55) | 515 (350) |
| $CH_3CN$ | 533 (20) | 518 (89) |
| DMSO | 535 (13) | 520 (38) |
| DMF | 538 (10) | 525 (17) |

[a] Excited at $\lambda_{ex} = 450$ nm.
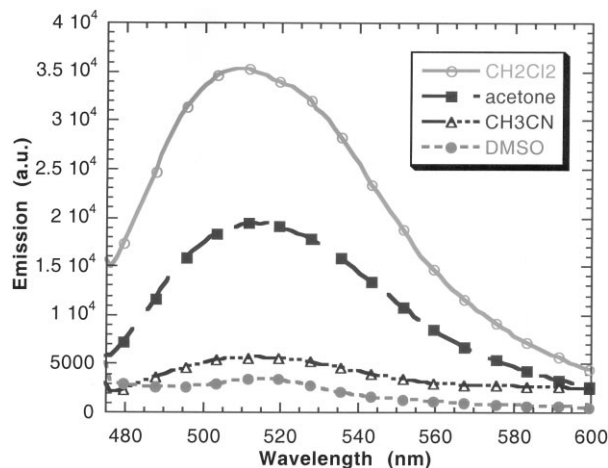


Fig. 6. Change of emission intensity of [(dppm)Pt(C$_2$P$_2$)]$_2$(OTf)$_4$ (2) in different solvents.
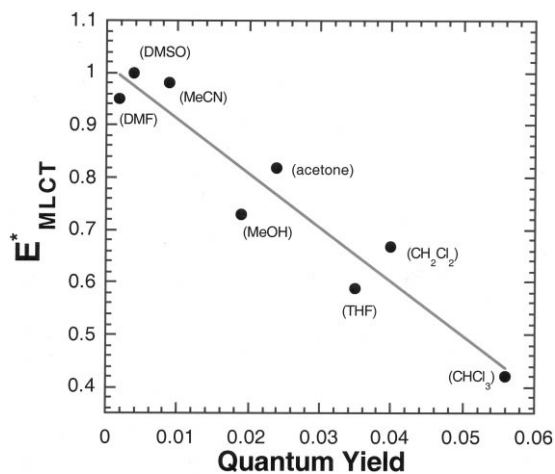
Fig. 7. Plot of $E^*_{MLCT}$ vs. quantum yields for [(dppm)Pt(C$_2$P$_2$)]$_2$(OTf)$_4$ (**2**).
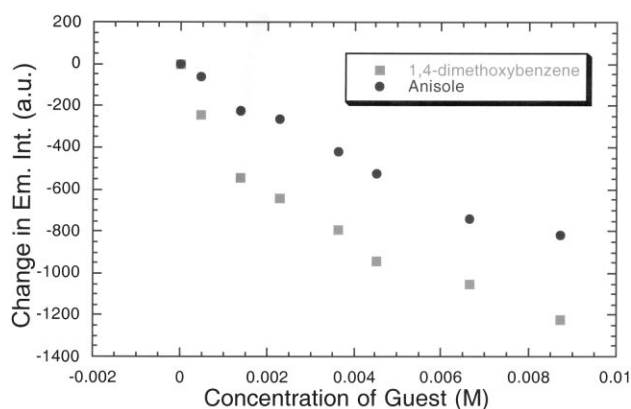


Fig. 8. Plot of net change of emission intensity (monitoring $\lambda_{em} = 512$ nm, $\lambda_{ex} = 450$ nm) of **2** vs. concentration of guest molecules.
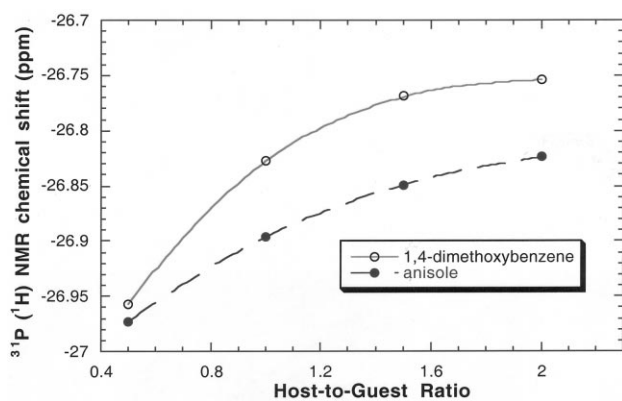


Fig. 9. Plot of the $^{31}$P{$^1$H}-NMR chemical shifts of [(dppm)Pd(C$_2$P$_2$)]$_2$(OTf)$_4$ (**1**) vs. host-to-guest ratio.

### 3.4. Host–guest chemistry

The investigation of the host–guest behavior of inorganic cyclophanes can be achieved using the NMR chemical shift [1,3] and/or changes in the excited-state emission intensity [2]. Both characteristics can be used in the investigation of our macrocyclic Pd(II)/Pt(II) species with C$_2$P$_2$ spacer. It was observed that the emission intensity of **2** ($\lambda_{em} = 512$ nm with excitation at 450 nm) decreases dramatically upon addition of the guest molecule anisole or 1,4-dimethoxybenzene in CH$_2$Cl$_2$. Here the guest molecules are chosen based on the cavity size of the host molecule (Pt-to-Pt distance is 7.2 Å). Fig. 8 displays the change of the emission intensity as a function of the concentration of guest molecules. As the guest concentration increases, the observed luminescence intensity of **2** decreases.

Binding studies were also performed to evaluate the relative strengths of association between the guest molecules and the host cavity. The decrease in emission at 512 nm was fit to a binding expression of the form [2d]

$$I = I_0 + (\Delta I^* K^*_b C)/(1 + K^*_b C) \tag{1}$$

Here, $C$ is the concentration of the guest molecule, $K_b$ is the host–guest binding constant, $I_0$ and $\Delta I$ are the initial luminescence intensity and the extrapolated maximum change in intensity at 512 nm, respectively. Eq. (1) is valid when the guest concentration is significantly higher than that of the host molecule, and the binding molecularity and stoichiometry are both 1:1 [2d,22]. The binding constants thus obtained for complex **2** are 309 M$^{-1}$ for guest molecule anisole (C$_6$H$_5$OCH$_3$) and 61 M$^{-1}$ for 1,4-dimethoxybenzene. Presumably the size of the guest molecule may play a role here in determining the magnitude of the binding constant, since the dimeric host molecule **2** has a relatively small cavity.

Efforts have been made to carry out a similar host–guest study using the emission property of the homobimetallic complex **1**, but it was thwarted by the much weaker emission intensity of this complex. Hence, $^{31}$P{$^1$H}-NMR analysis was used to probe the host–guest behavior of **1**. Upon addition of the guest molecule anisole or 1,4-dimethoxybenzene, the $^{31}$P{$^1$H}-NMR chemical shift of the auxiliary dppm ligand does not change. However, the chemical shift of C$_2$P$_2$ spacer shifts ca. 0.2 ppm when the host-to-guest ratio changes from 0.5 to 2 (Fig. 9). This observation suggests that the guest molecule may locate or insert into the ten-member ring consisting two C$_2$P$_2$ spacers and two Pd centers.

### 4. Conclusions

Luminescent monomeric and macrocyclic Pd(II)/Pt(II) dimeric complexes with Ph$_2$PC≡CPPh$_2$ have been prepared and characterized. The electronic absorption,

emission and quantum yields as well as their solvent dependence have been investigated. When the solvent polarity increases, the absorption band shifts to higher energy, and the emission maximum shifts to lower energy along with the decreased quantum yield. Several representative features can be summarized here. (a) The large differences in the absorption, emission and quantum yields between the Pd(II) and Pt(II) complexes suggest that the emitting excited states are not pure LLCT but involve metal-based orbitals. The observed solvatochromic effects in absorption, emission and quantum yields also rule out the possibility of intra-ligand or metal-centered emitting excited states. Previously Eisenberg and co-workers [19] have assigned $Pt(d_\pi)/S(P_\pi)$ to diimine $(\pi^*)$ CT state as the emitting excited state in the Pt–diimine–dithiolate system, and $Pt(d_\pi)$ to $S(P_\pi)$ CT excited state in the Pt–diphosphine–dithiolate system. In the study of the complex *trans*-[Pt(C≡C–Ph)$_2$(dppm–P)$_2$] Yam et al. [23] reported, based on the extended Hückel calculation, the assignment of an emissive excited state of large platinum-to-acetylide MLCT character, with substantial mixing of the $\pi^*$ orbital of phenylacetylide with the $6p_z$ orbital of Pt and of the $5d_{yz}$(Pt) orbital with the $\pi$(C≡C–Ph) orbitals. Metal-to-ligand charge transfer $(nd_{z2} \to \pi_L)$ with some admixture of $(n+1) P_z$ orbital in $\pi_L$ was also assigned as the lowest excited state of Rh(I)/Ir(I) diphosphine systems by Fordyce and Crosby [24]. For our Pd and Pt systems, large absorption coefficients were observed for the CT bands (Table 4). Hence, we may conclude that the emitting excited state in our complexes with auxiliary dppm and C$_2$P$_2$ spacer is the MLCT/LLCT admixture. Other excited states of different orbital character may lie close in energy, including intraligand and metal-centered state. The mixing between the emitting excited state with the non-emissive upper excited state may account for the short lifetimes (1–3.6 ns) observed in our systems. (b) Excellent correlation was observed between the $E^*_{\text{MLCT}}$ solvent scale and the absorption maximum or quantum yield of complexes **1** and **2**. (c) The Pt(II) complexes have much higher quantum yields when compared with the Pd(II) complexes. Presumably this can be ascribed to the heavy atom effect in the spin–orbit coupling which results in the increase of intensity of transition from the ${}^3$MLCT exciting state to the singlet ground state. (d) From host–guest study, binding constants of 309 and 61 M$^{-1}$ were calculated for anisole and 1,4-dimethoxybenzene guests, respectively, when macrocyclic complex **2** was used as the host molecule. Currently the preparation and properties of the macrocyclic complexes with longer sp carbon chains are under investigation.

## 5. Supplementary material

Crystallographic data for the structural analysis have been deposited with the Cambridge Crystallographic Data Centre, CCDC no. 133906. Copies of this information may be obtained free of charge from The Director, CCDC, 12 Union Road, Cambridge, CB2 1EZ, UK (Fax: + 44-1223-336033; e-mail: deposit@ccdc.cam.ac.uk or www: http://www.ccdc.cam.ac.uk).

## References

[1] (a) P.J. Stang, B. Olenyuk, Acc. Chem. Res. 30 (1997) 502, and references cited therein. (b) P.J. Stang, D.H. Cao, S. Saito, A.M. Arif, J. Am. Chem. Soc. 117 (1995) 6273. (c) B. Olenyuk, J.A. Whiteford, P.J. Stang, J. Am. Chem. Soc. 118 (1996) 8221. (d) J.A. Whiteford, E.M. Rachlin, P.J. Stang, Angew. Chem. Int. Ed. Engl. 35 (1996) 2524. (e) P.J. Stang, B. Olenyuk, Angew. Chem. Int. Ed. Engl. 35 (1996) 732. (f) P.J. Stang, J.A. Whiteford, Res. Chem. Intermed. 22 (1996) 659.

[2] (a) R.V. Slone, D.I. Yoon, R.M. Calhoun, J.T. Hupp, J. Am. Chem. Soc. 117 (1995) 11 813. (b) R.V. Slone, J.T. Hupp, C.L. Stern, T.E. Albrecht-Schmitt, Inorg. Chem. 35 (1996) 4096. (c) K.D. Benkstein, J.T. Hupp, C.L. Stern, Inorg. Chem. 37 (1998) 5404. (d) R.V. Slone, K.D. Benkstein, S. Bélanger, J.T. Hupp, I. Guzei, A.L. Rheingold, Coord. Chem. Rev. 171 (1998) 221.

[3] (a) M. Fujita, J. Yazaki, K. Ogura, J. Am. Chem. Soc. 112 (1990) 5645. (b) M. Fujita, O. Sasaki, T. Mitsuhashi, T. Fujita, J. Yazaki, K. Yaaguchi, K. Ogura, Chem. Commun. (Cambridge) (1996) 1535. (c) M. Fujita, S. Nagao, M. Iida, K. Ogata, K. Ogura, J. Am. Chem. Soc. 115 (1993) 1574.

[4] J.R. Farrell, C.A. Mirkin, I.A. Guzei, L.M. Liable-Sands, A.L. Rheingold, Angew. Chem. Int. Ed. Engl. 37 (1998) 465.

[5] (a) F.M. Romero, R. Ziessel, A. Dupont-Gervais, A. Vandorsselaer, Chem. Commun. (Cambridge) (1996) 551. (b) A.J. Carty, A. Efraty, Can. J. Chem. 47 (1969) 47 2573. (c) W. Oberhauser, C. Bachmann, T. Stampfl, P. Brüggeller, Inorg. Chim. Acta. 256 (1997) 223. (d) H.C. Clark, G. Ferguson, P.N. Kapoor, M. Parvez, Inorg. Chem. 24 (1985) 3924.

[6] S.M. Woessner, J.B. Helms, Y. Shen, B.P. Sullivan, Inorg. Chem. 37 (1998) 5406.

[7] E.C. Constable, E. Schofield, Chem. Commun. (Cambridge) (1998) 403.

[8] C.M. Drain, J.-M. Lehn, J. Chem. Soc. Chem. Commun. (1994) 2313.

[9] P.N.W. Baxter, Metal ion directed assembly of complex molecular architectures and nanostructures, in: J.-M. Lehn, J.P. Sauvage, M.W. Hosseni, Comprehensive Supramolecular Chemistry, vol. 9, Ch. 5, Pergamon, Oxford, 1996.

[10] (a) M. Fujita, Coord. Chem. Rev. 148 (1996) 249. (b) M. Fujita, Synth. J. Org. Chem. Jpn. 54 (1996) 953.

[11] (a) F.A. Cotton, B. Hong, M. Shang, G.G. Stanley, Inorg. Chem. 32 (1993) 3620. (b) F.A. Cotton, B. Hong. Progress in Inorganic Chemistry, Vol. 40, Wiley, New York, 1992, p. 179, and references cited therein. (c) B. Hong, J.V. Ortega, Angew. Chem. Int. Ed. Engl. 37 (1998) 2131. (d) F.A. Cotton, B. Hong, Inorg. Chem. 32 (1993) 2354.

[12] (a) E.M. Kober, B.P. Sullivan, W.J. Dressick, J.V. Caspar, T.J. Meyer, J. Am. Chem. Soc. 102 (1980) 7383. (b) R.G. Brewer, G.E. Jensen, K.J. Brewer, Inorg. Chem. 33 (1994) 124. (c) P.-W. Wang, M.A. Fox, Inorg. Chem. 34 (1995) 36.

[13] C. Charrier, P. Chodkiewicz, W. Cadiot, Memoires Presentés a La Société Chimique, 1965, p. 1002.

[14] (a) SMART Software Users Guide, Version 4.21, Bruker Analytical X-Ray Systems, Inc., Madison,WI, 1997. (b) SAINT Software Users Guide, Version 4.05, Bruker Analytical X-Ray Systems, Inc., Madison, WI 1997. (c) G.M. Sheldrick, SADABS, Bruker Analytical X-Ray Systems, Inc., Madison, WI, 1997. (d) G.M. Sheldrick, SHELXTL Version 5.10, Bruker Analytical X-Ray Systems, Inc., Madison, WI, 1997. (e) International Tables for X-Ray Crystallography, Vol. C, Kluwer, Dordrecht, 1992.

[15] (a) D.A. Buckingham, F.P. Dwyer, H.A. Goodwin, A.M. Sargeson, Aust. J. Chem. 17 (1964) 325. (b) E.M. Kober, J.V. Casper, B.P. Sullivan, T.J. Meyer, Inorg. Chem. 27 (1988) 4587.

[16] F. Barigelletti, L. Flamigni, V. Balzani, J.-P. Collin, J.-P. Sauvage, A. Sour, E.C. Constable, A.M.W.C. Thompson, J. Am. Chem. Soc. 116 (1994) 7692.

[17] (a) C.K. Ryu, R.H. Schmehl, J. Phys. Chem. 93 (1989) 7961. (b) L. De Cola, V. Balzani, F. Barigelletti, L. Flamigni, P. Belser, A. von Zelewsky, M. Frank, F. Vögtle, Inorg. Chem. 32 (1993) 5228.

[18] N. Sutin, Acc. Chem. Res. 15 (1982) 275.

[19] (a) J.A. Zuleta, J.M. Bevilacqua, J.M. Rehm, R. Eisenberg, Inorg. Chem. 31 (1992) 1332. (b) J.A. Zuleta, J.M. Bevilacqua, D.M. Proserpio, P.D. Harvey, R. Eisenberg, Inorg. Chem. 31 (1992) 2396. (c) J.M. Bevilacqua, J.A. Zuleta, R. Eisenberg, Inorg. Chem. 33 (1994) 258. (d) S.D. Cummings, R. Eisenberg, J. Am. Chem. Soc. 118 (1996) 1949.

[20] T.R. Lakowicz, Principles of Fluorescence Spectroscopy, Plenum Press, New York, 1983, pp. 187–201.

[21] D.M. Manuta, A.J. Lees, Inorg. Chem. 22 (1983) 3825.

[22] M.D. Todd, Y. Dong, J. Horney, D.I. Yoon, J.T. Hupp, Inorg. Chem. 32 (1993) 2001.

[23] V.W.-W. Yam, K.K.-W. Lo, K.M.-C. Wong, J. Organomet. Chem. 578 (1999) 3.

[24] W.A. Fordyce, G.A. Crosby, Inorg. Chem. 21 (1982) 1455.